ISSN 0031-918X, Physics of Metals and Metallography, 2023, Vol. 124, No. 7, pp. 734–741. © Pleiades Publishing, Ltd., 2023.
Russian Text © The Author(s), 2023, published in Fizika Metallov i Metallovedenie, 2023, Vol. 124, No. 7, pp. 660–667.

STRENGTH AND PLASTICITY

Structural Evolution of 10% Cr–3% Co Steel Microalloyed with Re and Cu during Creep at 923 K

A. E. Fedoseeva*

Belgorod National Research University, Belgorod, 308015 Russia

**e-mail: fedoseeva@bsu.edu.ru*

Received August 31, 2022; revised May 24, 2023; accepted June 12, 2023

Abstract—Structural evolution of the tempered lath martensite of the 10% Cr–3% Co steel microalloyed with rhenium and copper with a low nitrogen content and a high boron content during creep at 923 K was investigated for the purpose of establishment of the rison of decrease in creep resistance of this steel under the low applied stress. The tempered martensite lath structure of 10% Cr–3% Co steel with an average lath size of 370 nm and a high dislocation number density of 2×10^{14} m^{-2} was observed after normalizing at 1323 K with the following tempering at 1043 K for 3 h. The structure was stabilized by $M_{23}C_6$ carbides, M_6C carbides, and NbX carbonitrides. During long-term creep, the lath structure strongly experienced an evolution: the width of the martensitic laths increased significantly, dislocation density decreased, the Laves phase and Cu-enriched particles remarkably coarsen. Such structural evolution correlates with an appearance of creep strength breakdown on curves "Applied stress *vs.* Time to failure" and "Minimum creep rate *vs.* Applied stress". Significant coarsening of the Laves phase particles and Cu-enriched particles via formation of the large particles with sizes more than 250 nm along high-angle boundaries and full dissolution of the fine particles with sizes less than 50 nm along low-angle boundaries of martensite laths is considered to be the main cause of degradation of the creep resistance of the steel studied.

Keywords: creep-resistant martensitic steel, heat treatment, creep, microstructure, secondary phase particles, softening

DOI: 10.1134/S0031918X23601038

INTRODUCTION

The strategic direction for the development of the heat and power industry operating on solid fuels is the creation of steam turbine power units of a new generation operating at ultra-supercritical steam parameters (USSP) of T = 873–893 K, P = 250–300 atmospheres, having a perfect flow part and improved thermal scheme [1, 2]. Currently, coal-fired thermal power plants in Russia, operating at steam parameters of 818–833 K and 140–240 atmospheres, have exhausted their resource and must be replaced. They have a low efficiency (34–37%) and large harmful emissions into the atmosphere. By increasing the steam parameters to USSP, it is planned to increase the efficiency up to 41–44% and reduce harmful thermal emissions [1]. In the Russian Federation, currently there are no materials that meet the requirements for a new generation of power equipment.

High-chromium martensitic steels can be considered as a material for the manufacture of elements of boilers and steam pipelines, as well as blades and rotors of steam turbines for thermal power plants operating at USSP [1, 2]. These steels are a complexly alloyed material, in which each alloying element is justified and performs a strictly assigned function [3–8]. The structure of such steels after heat treatment is a hierarchical system, where the prior austenite grains (PAGs) are divided into packets (a group of laths with the same habit plane), which are divided into blocks consisting of martensite laths of the same orientation, while the structure contains a high density of dislocations inside laths [9–11]. Most misorientations of the boundaries of packets and blocks that satisfy the Kurdjumov–Sachs orientation relationship exceed 15°, which is usually the criterion between low-angle and high-angle boundaries. Even the minimum misorientation, 10.53°, is relatively high, while the misorientations between individual laths are low-angle boundaries within a few degrees, usually not exceeding 5° [9, 10]. Such a complex hierarchical structure is stabilized by various types of secondary phase particles [4].

The content of 9–10% Cr provides high hardenability of steel, and chromium also participates in the formation of grain-boundary $M_{23}C_6$ carbides, which prevent the migration of low-angle boundaries during creep [3, 4]. The addition of boron in an amount of 0.008–0.012 wt % leads to partial replacement of carbon atoms in the $M_{23}C_6$ carbide by boron atoms with the formation of the $M_{23}(C,B)_6$ phase that reduces the average size of this phase and increases its number

Table 1. The chemical composition of the steels studied (in wt %)

Ingot	C	Cr	Co	Mo	W	V	Nb	B	N	Cu	Re
10%Cr–3Co–2W–0.8Cu	0.09	9.7	3.2	0.5	2.0	0.2	0.05	0.015	0.002	0.8	0.2
10%Cr–3Co–3W–0.2Cu	0.11	9.9	3.1	0.1	2.9	0.2	0.07	0.008	0.002	0.2	0.2

density along the low-angle boundaries of martensite laths [4, 7]. Carbon in an amount from 0.02 to 0.1 wt % and nitrogen in an amount from 0.003 to 0.05% together with 0.20% vanadium and 0.05% niobium provide the formation of MX carbonitrides, where M means V, Nb or a combination of them, and X is C, N or a combination of them [3, 4, 8, 12]. MX particles serve as obstacles to the movement of free dislocations and their rearrangement into low-energy configurations [3, 4, 8, 12]. In steels with a high nitrogen content, these particles act as the main sources of threshold stresses; however, due to their thermodynamic instability, MN nitrides tend to transform into large Z-phase (Cr(V,Nb)N) particles, which sharply reduces the creep resistance of high-chromium steels, despite the retaining MC carbides [5, 12]. In steels with a low nitrogen content, the volume fraction of MN nitrides is low, which eliminates the opportunity of the large Z-phase particles formation, but, on the other hand, deprives the steel of the main source of strengthening via disperssion hardening [7].

Of particular importance are elements that provide effective solid-solution strengthening and slowing down diffusion processes during creep. These elements include cobalt, tungsten, molybdenum, and rhenium [5, 13]. At the same time, tungsten and molybdenum are prone to the formation of the Laves-phase particles ($Fe_2(W,Mo)$), which, on the one hand, prevent the migration of the lath boundaries during the primary creep stage, but, on the other hand, have a tendency to strong coarsening that reduces the creep resistance due to the occurrence of crack sources [4]. An interesting position is taken by the addition of rhenium, since this element significantly increases the creep resistance of the steel by reducing the diffusion of the iron and tungsten atoms, but at the same time does not affect the solubility of tungsten in the ferrite matrix, as it was supposed in original research [13].

In previous studies for the rhenium-containing 10% Cr–3% Co–3% W steel [7, 13], it was demonstrated uniquely high lifetimes to rupture of 10000 h for creep test at 923 K under 140 MPa [7, 13]. However, for this steel, a creep strength breakdown was found [7], the creep resistance decreased remarkably under the applied stresses below 140 MPa. This led to the development of a new modified composition of rhenium-containing 10% Cr–3% Co steel by changing the ratio of tungsten and molybdenum, as well as the addition of 0.8% copper. Copper is introduced to form nanoclusters, which are the nucleation sites for the Laves-phase particles [3]. The aim of the present study was to identify the effect of modification of the chemical composition of Re-containing 10% Cr steel on creep resistance at a temperature of 923 K.

EXPERIMENTAL

The Re-containing steels, designated here as 10% Cr–3Co–2W–0.8Cu (new modified composition) and 10% Cr–3Co–3W–0.2Cu (the steel for comparison), the chemical composition of which is presented in Table 1, were melted in a vacuum induction furnace in the amount of 40 kg. The ingots were homogenized at a temperature of 1473 K and forged at temperatures of 1373–1423 K. The heat treatment of the steels studied was the same and consisted of normalizing at a temperature of 1323 K for 1 hour, cooling in air, followed by tempering at a temperature of 1043 K for 3 hours, air cooling. Creep tests were carried out using the flat samples with a cross section of 7×3 mm and a gauge length of 25 mm at a temperature of 923 K under the applied stresses from 200 to 100 MPa with a step of 20 MPa. Structural studies were carried out in the area of uniform elongation of ruptured specimens using a JEOL JEM-2100 transmission electron microscope (TEM) with an INCA energy dispersive spectrometer and an FEI Quanta 600 FEG scanning electron microscope (SEM). More details of sample preparation for TEM and SEM, as well as analysis of structural elements, you can find in Refs. [5, 7, 8, 12, 13].

RESULTS AND DISCUSSION

Structure after Heat Treatment

Figure 1 shows the initial structure of the 10% Cr–3Co–2W–0.8Cu steel after heat treatment. Structural parameters of steel are summarized in Table 2 in comparison with the 10% Cr–3Co–3W–0.2Cu steel. TEM revealed the formation of tempered martensite lath structure with an average transverse size of martensite laths of 370 ± 30 nm in the 10% Cr–3Co–2W–0.8Cu steel (Fig. 1a). A high dislocation density inside lath interiors, which was determined by the count of dislocation points on the upper and lower surfaces of the foil by TEM, of about 2.1×10^{14} m^{-2} was found.

The boundaries of the lath structure were decorated by $M_{23}C_6$ carbides with an average size of 70 ± 7 nm (Figs. 1b, 1d, Table 2). These particles were enriched in Cr, Fe, and W, and their average chemical composition was (in wt %) (40–43)% Cr–(17–18)% Fe–(0.2–0.5)% Mo–(40–41)%W. The particle num-

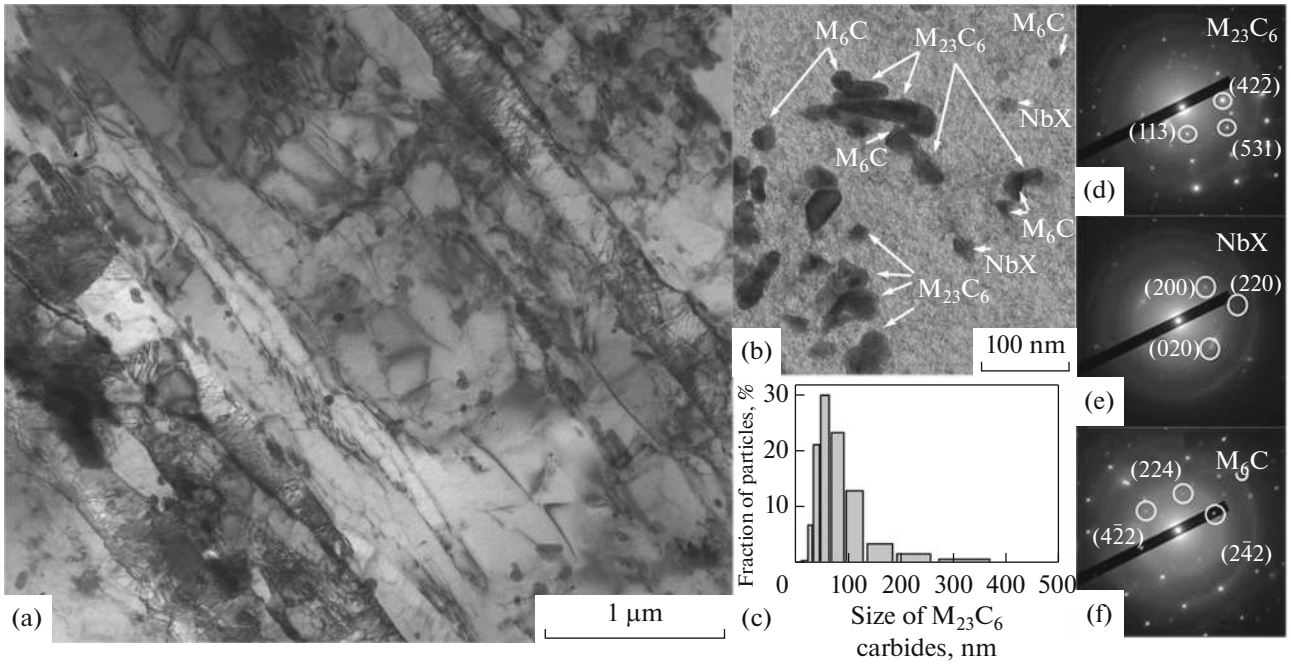

Fig. 1. (a, b) TEM images of microstructure of the 10% Cr–3Co–2W–0.8Cu steel after heat treatment together with images of the (b) secondary phase particles with corresponding electron diffraction patterns for carbides of (d) $M_{23}C_6$, (e) M_6C, and carbonitrides (f) NbX, as well as (c) size distribution of $M_{23}C_6$ carbides.

ber density of $M_{23}C_6$ carbides along the high-angle boundaries of PAGs, packets and blocks, and low-angle boundaries of the martensite laths, estimated using TEM images, is 5.1 and 2.6 μm^{-1}, respectively. It should be noted that high fraction of fine particles with sizes less than 20 nm was located along the low-angle boundaries of martensite laths. On the contrary, very large particles with sizes more than 300 nm were precipitated at the high-angle boundaries, while no such particles were found at the low-angle boundaries. In general, it can be noted that the fraction of particles with sizes ranging from 50 to 70 nm was about 30% (Fig. 1c). In general, the fraction of coarse particles with sizes more than 150 nm did not exceed 5% (Fig. 1c). Inside the martensitic laths, uniformly distributed NbX particles having round shape and chemical composition (in wt %) of 1% V–15% Cr–5% Fe–79% Nb were observed. The average size of NbX particles was 29 ± 4 nm (Figs. 1b, 1e). Along the low-angle boundaries of martensite laths, non-equilibrium particles of M_6C carbides having round shape with an average size of 40 ± 4 nm were also found (Figs. 1b, 1f). The average chemical composition of such particles was (in wt %) 22% Cr–(6–10)% Fe–(68–72)% W. The volume fractions of the last two phases, estimated using the Thermo-Calc software, were negligible in the 10% Cr–3Co–2W–0.8Cu steel, therefore, they were not considered further. Note that the phase compositions of the steels studied coincided [13]. The structural parameters of both steels were also similar (Table 2). Significant differences were lower volume fractions of the $M_{23}C_6$ carbides and NbX carbonitrides, as well as a larger size of PAGs and width of martensitic laths in 10% Cr–3Co–2W–0.8Cu steel.

Creep Behavior at 923 K

Figure 2 shows the dependences of "Applied stress vs. Rupture time" and "Minimum creep rate vs. Applied stress" for creep tests at 923 K for the

Table 2. Structural parameters of the steels studied after heat treatment

Ingot	PAG size, μm	Lath width, nm	Dislocation density, m^{-2}	Secondary phase particles			
				$M_{23}C_6$		NbX	
				size, nm	fraction, %	size, nm	fraction, %
10% Cr–3Co–2W–0.8Cu	62 ± 5	370 ± 30	2.1×10^{14}	72 ± 10	1.56	40 ± 5	0.056
10% Cr–3Co–3W–0.2Cu	55 ± 5	290 ± 30	2.0×10^{14}	67 ± 10	1.98	40 ± 5	0.078

10% Cr–3Co–2W–0.8Cu steel in comparison with the 10% Cr–3Co–3W–0.2Cu steel. Under the high applied stresses, 10% Cr–3Co–2W–0.8Cu steel had a significant increase in rupture time, which was 8, 4, and 10 times compared to the 10% Cr–3Co–3W–0.2Cu steel under the applied stresses of 200, 180, and 160 MPa, respectively. In this case, the slope of the long-term strength curves for both steels in the region of high stresses was the same and amounted to 0.053 MPa/h (Fig. 2a). Thus, a decrease in the content of tungsten to 2% with an addition of 0.8% copper favorably affects the short-term creep. Note that both steels demonstrated the creep strength breakdown after 4000 hours of creep testing. This led to an increase in the slope of the creep strength curve to 0.28 MPa/h (Fig. 2a), although the test under 100 MPa for steel 10% Cr–3Co–2W–0.8Cu has not yet been completed, it is expected that the rupture time of this steel will be comparable with the 10% Cr–3Co–3W–0.2Cu steel (Fig. 2a). In the region of low applied stresses, the behavior of both steels was similar, which indicated a similar microstructural evolution in these steels.

The relationship between the minimum creep rate and the applied stresses was linear. The experimental data obey the power law of creep over the entire range of applied stresses in the form [2, 3]:

$$\dot{\varepsilon}_{\min} = A\sigma^{n^*} \exp\left(-\frac{Q}{RT}\right), \quad (1)$$

where $\dot{\varepsilon}_{\min}$ is the minimum creep rate, σ is the applied stress, Q is the activation energy for plastic deformation, R is the gas constant, T is the temperature, A is a constant, n^* is the "apparent" exponent. It can be seen that the curves in Fig. 2b for the 10% Cr–3Co–2W–0.8Cu and 10% Cr–3Co–3W–0.2Cu steels had an inflection points at the applied stresses of 160 and 140 MPa, respectively. For the 10% Cr–3Co–2W–0.8Cu and 10% Cr–3Co–3W–0.2Cu steels, the curves in Fig. 2b provided the best linear fit for the "apparent" exponent in the plastic deformation equation $n^* = 27$ and 23 at the applied stresses ranging from 200 to 160 and from 200 to 140 MPa, respectively, and $n^* = 6$ under the applied stresses ranging from 160 to 120 MPa and $n^* = 4.5$ under the applied stresses ranging from 140 to 120 MPa, respectively (Fig. 2b).

Estimation of threshold stresses by simple extrapolation of the curve to the abscissa corresponding to the minimum creep rate of 10^{-11} s^{-1} [14] showed that for the 10% Cr–3Co–2W–0.8Cu and 10% Cr–3Co–3W–0.2Cu steels, the values of the threshold stresses amounted to 138 and 115 MPa, respectively, for the region of high stresses, and 85 and 69 MPa, respectively, for the region of low applied stresses. The dependence of "Minimum creep rate vs. Effective stress", defined as the difference between the applied and threshold stress, was plotted in the aim to establish the true exponents in the plastic deformation equation

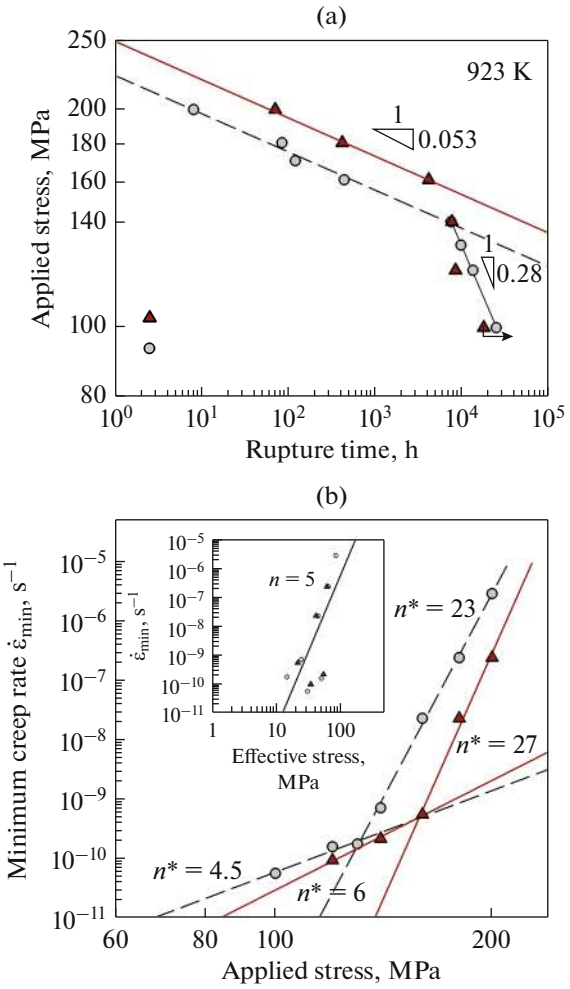

Fig. 2. The dependences of (a) "Applied stress vs. Rupture time" and (b) "Minimum creep rate vs. Applied stress" for creep tests at 923 K for the 10% Cr–3Co–2W–0.8Cu steel (▲). For comparison the data for 10% Cr–3Co–3W–0.2Cu steel were added (●).

for both steels (Fig. 2b). The true stress exponent n for both studied steels was 5.3 for the entire range of the applied stresses, which was close to $n = 5$ and indicated creep controlled by high-temperature dislocation climbing via lattice diffusion [15] without any change in the deformation mechanism.

Structure after Creep

Analysis of the structural evolution of the 10% Cr–3Co–2W–0.8Cu steel after creep using TEM of foils and carbon replicas, as well as Z-contrast (SEM) found a significant increase in the transverse size of martensitic laths and a decrease in dislocation number density in the area of uniform elongation for tests under applied stresses below 160 MPa (Fig. 3) that correlated with the appearance of creep strength breakdown (Fig. 2a). Thus, the width of martensite

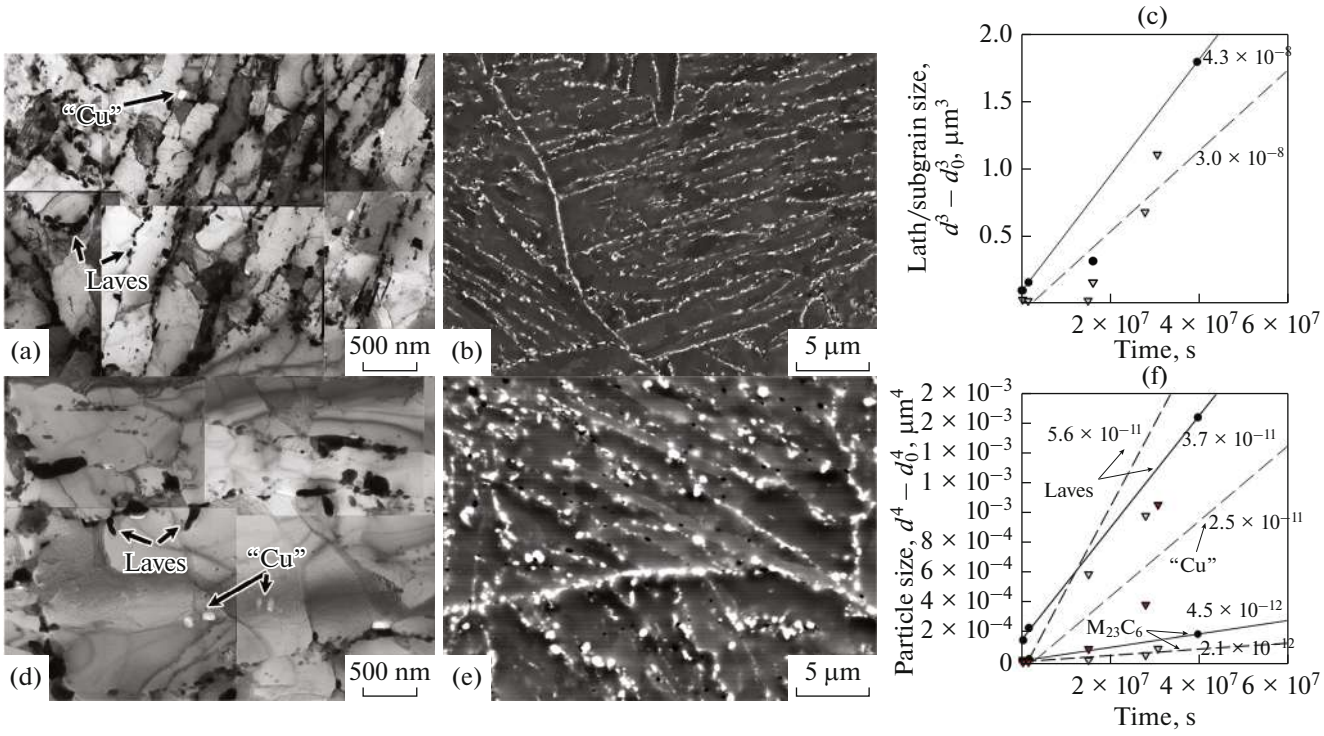

Fig. 3. (a, d) TEM and (b, e) SEM images for the 10% Cr–3Co–2W–0.8Cu steel after creep tests at 923 K under the applied stresses of (a, b) 180 MPa and (d, e) 120 MPa together with the (c) time dependence of the transverse size of martensite laths and (f) secondary phase particles. Numbers in (c, f) indicate the coarsening rate constant k for the (▽ and ▼) 10%Cr–3Co–2W–0.8Cu steel, (●) 10% Cr–3Co–3W–0.2Cu steel.

laths increased from 300 nm in the region of high applied stresses (Fig. 3a) to about 1 μm in the region of the low applied stresses (Fig. 3d). Dislocation number density reduced from 2×10^{14} m^{-2} in the region of the high applied stresses to 0.6×10^{14} m^{-2} in the region of the low applied stresses.

For both steels, during creep the precipitation of the Laves-phase particles with an average chemical composition (in wt %) (10–20)% Cr–(20–30)% Fe–(50–70)% W along the high-angle boundaries of the PAGs, blocks and packets, as well as along the low-angle boundaries of the martensitic laths was revealed. Figures 3b, 3e showed that the Laves-phase particles, which looks like the white particles in SEM images, became significantly larger with decreasing applied stress, whereas their number particle density decreased. $M_{23}C_6$ carbide did not significantly change during long-term creep. A distinctive feature of 10% Cr–3Co–2W–0.8Cu steel comprised the precipitation of Cu-enriched particles, which looks like the white particles in TEM images (Figs. 3a, 3d). The equilibrium volume fractions of the Laves-phases and Cu-enriched particles were 1.8 and 1.5%, respectively, and were achieved after the first 500 hours of creep tests at 923 K [7].

An analysis of the coarsening of martensitic laths together with coarsening of $M_{23}C_6$ carbides, Laves-phase and Cu-enriched particles was made suggesting that coarsening occurred according to the Ostwald mechanism and could be described by the Lifshitz–Slyozov–Wagner equation [16, 17]:

$$d^m - d_0^m = k(t - t_0), \quad (2)$$

where d_0 and d are the average sizes of laths/particles over the time t_0 and t, respectively, k is the coarsening rate constant, the coefficient m depends on the mechanism of coarsening ($m = 3$ for bulk diffusion and $m = 4$ for grain boundary diffusion).

Figures 3c and 3f showed time changes in the sizes of martensite laths, as well as secondary phase particles. For comparison, data for the 10% Cr–3Co–3W–0.2Cu steel were given. During creep, the coarsening rate constant of the martensitic laths in the 10% Cr–3Co–2W–0.8Cu steel was 1.5 times lower than in the 10% Cr–3Co–3W–0.2Cu steel. The growth of martensitic laths due to the migration of the triple junction was restrained by grain boundary particles, which were the sources of the Zener retarding forces. The smaller the particles and the smaller the distance between them, the more effective is the Zener retarding force [18]. The lower value of coarsening rate constant of martensitic laths in the 10% Cr–3Co–2W–0.8Cu steel was caused by the lower coarsening rate constant of $M_{23}C_6$ carbides, which amounted to 2.1×10^{-12} μm^4 s^{-1}

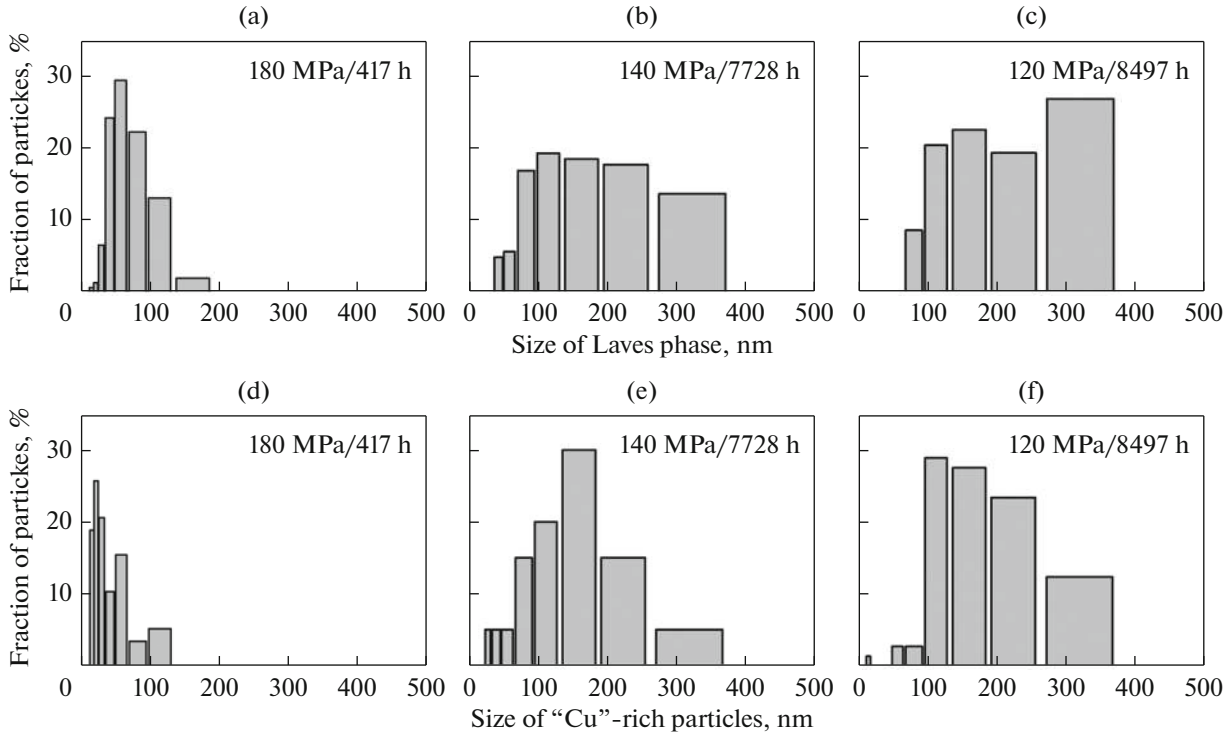

Fig. 4. Size distributions of (a–c) Laves-phase and (d–f) "Cu"-enriched particles in the 10% Cr–3Co–2W–0.8Cu steel after different creep tests at temperature of 923 K under the applied stresses of (a, d) 180, (b, e) 140, and (c, f) 120 MPa.

(Fig. 3f). It should be noted the high dimensional stability of $M_{23}C_6$ carbides in the 9–12% Cr steels with a high boron content [7], whose average size does not exceed 100 nm even after 10000 hours of creep at 923 K.

The coarsening rate constants of "Cu"-enriched particles, which were observed only in the steel with a high copper content, and the Laves-phase particles were an order of magnitude higher than those of $M_{23}C_6$ carbides for both steels (Fig. 3f). At the same time, the coarsening rate constant of Laves phase in the 10% Cr–3Co–2W–0.8Cu steel was 1.5 times higher than in the 10% Cr–3Co–3W–0.2Cu steel. It should be noted that the higher growth rate of the Laves-phase particles together with the growth of "Cu"-enriched particles did not provoke a higher rate of coarsening of the martensite laths, while retaining the fine average size of $M_{23}C_6$ carbides did not prevent the formation of subgrains and wide laths. The coarsening of martensite laths is more sensitive to the quantity of the number of fine particles located along low-angle boundaries and their dissolution than to the average size of all particles regardless of their location. To estimate the changes in the ratios between fine particles located along the low-angle boundaries and large particles located along the high-angle boundaries, the size distributions of the Laves-phase and "Cu"-enriched particles were plotted under various creep conditions, represented in Fig. 4.

Under the high applied stresses (up to the inflection point in Fig. 2a, more than 160 MPa), the size distributions of the Laves-phase particles and "Cu"-enriched particles were rather narrow (Figs. 4a, 4d). More than 30% of Laves particles and 75% of "Cu"-enriched particles with sizes to 50 nm located, mainly, along the low-angle boundaries of martensite laths (Figs. 4a, 4d). The fraction of particles larger than 150 nm did not exceed 2% (Figs. 4a, 4d).

As an applied stress decreased below 160 MPa, the size distributions of the Laves-phase and "Cu"-enriched particles became wider; the formation of the large particles with sizes more than 150 nm was observed (Figs. 4b, 4c, 4e, 4f). Decreasing the applied stresses led to the full dissolution of the Laves-phase particles with sizes less than 75 nm, which were located, mainly, along the low-angle boundaries of martensitic laths. Opposite, the fraction of large particles with sizes more than 250 nm increased from 5 to 25% (Figs. 4a–4c). Such large particles were located along high-angle boundaries (Fig. 3e). A similar situation was also observed for "Cu"-enriched particles. The main peak of these particles were also shifted to large sizes; the fraction of the large particles with sizes over 200 nm was more than 35%, whereas the fine particles almost completely disappeared (Figs. 4e, 4f). Thus, the appearance of creep strength breakdown and inflection points on curve of "Minimum creep rate vs. Applied stress" was accompanied with the sig-

nificant coarsening of the Laves-phase and "Cu"-enriched particles via dissolution of fine particles with sizes less than 50 nm located along low-angle boundaries that led to the significant growth of the martensitic laths even in a case of retaining $M_{23}C_6$ carbides with relatively fine sizes. Only a change in this alloying of the steel is not able to exclude the degradation of the creep resistance of 10% Cr steels with the low N content, therefore, further work will be aimed at changing the heat treatment of these steels [19].

CONCLUSIONS

The structural evolution of tempered martensite lath structure in the 10% Cr–3% Co steel microalloyed with rhenium and copper, with low nitrogen and high boron contents was investigated during creep at 923 K. It was found that under the high applied stresses up to 160 MPa, the 10% Cr–3Co–2W–0.8Cu steel demonstrates a significant increase in rupture time. However, as an applied stresses decrease, creep strength breakdown appears, like for 10% Cr–3Co–3W–0.2Cu steel, which indicates a decrease in creep resistance. Such degradation of creep properties for both steels correlates with a significant increase in the transverse size of martensite laths and a decrease in the dislocation density. The growth of laths to sizes of about 1 μm in the 10% Cr–3Co–2W–0.8Cu steel is caused by the almost complete dissolution of the fine Laves-phase particles with sizes less than 50 nm, located along low-angle boundaries, together with a significant coarsening of "Cu"-enriched particles. Such changes in the structure are accompanied with a decrease in threshold stresses by a factor of 1.7 for both steels at transition from the high applied stresses to the low stresses. At the same time, the deformation creep mechanism during long-term creep is high-temperature climb of dislocations via lattice diffusion.

ACKNOWLEDGMENTS

Author thanks the Joint Research Center of Belgorod State National Research University "Technology and Materials", the activity of which was supported from the Ministry of Science and Higher Education of the Russian Federation within the framework of agreement no. 075-15-2021-690, for using the equipment.

FUNDING

The work was financially supported by Russian Science Foundation (no. 19-73-10089-П, https://rscf.ru/en/project/19-73-10089/).

CONFLICT OF INTEREST

The author declares that she has no conflicts of interest.

REFERENCES

1. F. Abe, T.-U. Kern, and R. Viswanathan, *Creep-Resistant Steels* (Woodhead, Cambridge, 2008). https://doi.org/10.1533/9781845694012
2. R. O. Kaybyshev, V. N. Skorobogatykh, and I. A. Shchenkova, "New martensitic steels for fossil power plant: Creep resistance," Phys. Met. Metallogr. **109**, 186–200 (2010). https://doi.org/10.1134/s0031918x10020110
3. R. L. Klueh, "Elevated-temperature ferritic and martensitic steels and their application to future nuclear reactors," Int. Mater. Rev. **50**, 287–310 (2005). https://doi.org/10.1179/174328005X41140
4. F. Abe, "Precipitate design for creep strengthening of 9% Cr tempered martensitic steel for ultra-supercritical power plants," Sci. Technol. Adv. Mater. **9**, 013002 (2008). https://doi.org/10.1088/1468-6996/9/1/013002
5. A. E. Fedoseeva, P. A. Kozlov, V. A. Dudko, V. N. Skorobogatykh, I. A. Shchenkova, and R. O. Kaibyshev, "Microstructural changes in steel 10Kh9V2MFBR during creep for 40000 hours at 600°C," Phys. Met. Metallogr. **116**, 1047–1056 (2015). https://doi.org/10.1134/s0031918x15080049
6. V. V. Sagaradze, T. N. Kochetkova, N. V. Kataeva, K. A. Kozlov, V. A. Zavalishin, N. F. Vil'danova, V. S. Ageev, M. V. Leont'eva-Smirnova, and A. A. Nikitina, "Structure and creep of Russian reactor steels with a BCC structure," Phys. Met. Metallogr. **118**, 494–506 (2017). https://doi.org/10.1134/s0031918x17050131
7. A. Fedoseeva, I. Nikitin, E. Tkachev, R. Mishnev, N. Dudova, and R. Kaibyshev, "Effect of alloying on the nucleation and growth of laves phase in the 9–10% Cr–3% Co martensitic steels during creep," Metals **11**, 60 (2021). https://doi.org/10.3390/met11010060
8. A. E. Fedoseeva and S. I. Degtyareva, "The effect of prolonged annealing on the structural stability of nanoparticle-hardened low-carbon 9% Cr–3% Co steel," Phys. Met. Metallogr. **123**, 1041–1047 (2022). https://doi.org/10.1134/S0031918X22600889
9. S. Morito, H. Tanaka, R. Konishi, T. Furuhara, and T. Maki, "The morphology and crystallography of lath martensite in Fe–C alloys," Acta Mater. **51**, 1789–1799 (2003). https://doi.org/10.1016/s1359-6454(02)00577-3
10. S. Morito, Y. Adachi, and T. Ohba, "Morphology and crystallography of sub-blocks in ultra-low carbon lath martensite steel," Mater. Trans. **50**, 1919–1923 (2009). https://doi.org/10.2320/matertrans.mra2008409
11. V. M. Gundyrev, V. I. Zeldovich, and V. M. Schastlivtsev, "Crystallographic analysis and mechanism of martensitic transformation in Fe alloys," Phys. Met. Metallogr. **121**, 1045–1063 (2020). https://doi.org/10.1134/S0031918X20110046
12. V. A. Dudko, A. E. Fedoseeva, A. N. Belyakov, and R. O. Kaibyshev, "Influence of the carbon content on the phase composition and mechanical properties of P92-type steel," Phys. Met. Metallogr. **116**, 1165–1174 (2015). https://doi.org/10.1134/s0031918x15110058

13. A. Fedoseeva, I. Nikitin, N. Dudova, and R. Kaibyshev, "On effect of rhenium on mechanical properties of a high-Cr creep-resistant steel," Mater. Lett. **236**, 81–84 (2019). https://doi.org/10.1016/j.matlet.2018.10.081

14. Y. Li and T. G. Langdon, "A simple procedure for estimating threshold stresses in the creep of metal matrix composites," Scr. Mater. **36**, 1457–1460 (1997). https://doi.org/10.1016/s1359-6462(97)00041-9

15. F. A. Mohamed, K.-T. Park, and E. J. Lavernia, "Creep behavior of discontinuous SiC-Al composites," Mater. Sci. Eng., A **150**, 21–35 (1992). https://doi.org/10.1016/0921-5093(90)90004-m

16. I. Lifshitz and V. Slyozov, "The kinetics of precipitation from supersaturated solid solutions," J. Phys. Chem. Solids **19**, 35–50 (1961). https://doi.org/10.1016/0022-3697(61)90054-3

17. R. Wagner, R. Kampmann, and P. W. Voorhees, in *Homogeneous Second-Phase Precipitation* (Wiley, New York, 1991), pp. 213–303. https://doi.org/10.1002/9783527603978.mst0388

18. F. J. Humphreys and M. Hatherly, "Recrystallization of two-phase alloys," in *Recrystallization and Related Annealing Phenomena*, 2nd ed. (Pergamon, Oxford, 2004), pp. 285–319. https://doi.org/10.1016/B978-008044164-1/50013-X

19. A. E. Fedoseeva, I. S. Nikitin, and R. O. Kaibyshev, "Effect of the quenching temperature on the creep resistance of 9% Cr–1% W–1% Mo–V–Nb martensite steel," Phys. Met. Metallogr. **123**, 92–98 (2022). https://doi.org/10.1134/s0031918x22010033